



Observational Kinematic Characteristics of Blobs in Solar Coronal Helmet and Pseudo Streamers

Jae-Ok Lee¹, Kyung-Suk Cho^{1,2}, Junmo An³, Hwanhee Lee¹, Jungjoon Seough¹, Yeon-Han Kim¹, and Pankaj Kumar^{4,5}

¹ Korea Astronomy and Space Science Institute, 776 Daedeokdae-ro, Yuseong-gu, Daejeon, Republic of Korea

² Department of Astronomy and Space Science, University of Science and Technology, 776 Daedeokdae-ro, Yuseong-gu, Daejeon, Republic of Korea

³ Department of Astronomy and Space Science, Kyung Hee University, 1732, Deogyong-daero, Giheung-gu, Yongin-si, Gyeonggi-do, Republic of Korea

⁴ Department of Physics, American University, Washington, DC 20016, USA

⁵ Heliophysics Science Division, NASA Goddard Space Flight Center, Greenbelt, MD 20771, USA

Received 2021 July 27; revised 2021 September 2; accepted 2021 September 4; published 2021 October 5

Abstract

We examine two helmet and two pseudo streamers (HSs and PSs) observed on 2018 and 2019. The HSs (PSs) have dark coronal cavities and stretched loop structures (twin coronal cavities and narrow plasma sheet) at their bases, which are well observed in K-Coronagraph (K-Cor). Their outer-corona structures (top of core, cusp, and stalk) are also clearly identified in LASCO-C2. By investigating LASCO-C2 images, we find the following characteristics. (1) Blobs persistently move outward along the centers of HSs and PSs as well as their legs until the base of a stalk. We also detect outward-moving blobs along their outsides. (2) Blobs along the HS centers formed below tops of cores ($\sim 2.6 R_{\odot}$), while the other HS and PS blobs might be generated below $2.0 R_{\odot}$. (3) HS blob speeds are generally similar to or smaller than the solar wind speed based on Parker's model, while PS ones are larger. (4) HS (PS) blob speeds along the streamer centers are slightly smaller (larger) than those along the streamer legs, might be explained by the expansion-factor model. The blob speeds inside streamer structures (centers and legs) are larger than outside ones closer to solar equator, similar to typical solar wind speed distributions at solar minimum. (5) Several blobs along the HS centers only show sudden speed jumps at streamer cusps. These might be caused by sunward tension forces of overlying stretched closed fields and/or bidirectional outflows by magnetic reconnections in the cusps.

Unified Astronomy Thesaurus concepts: [Solar coronal streamers \(1486\)](#)

1. Introduction

During total solar eclipses, conical-shaped structures with long thin rays are constantly observed. These structures are called coronal streamers, which usually contain single (or double) prominences, dark cavities, and arches at their bases (Newkirk 1967; Saito & Tandberg-Hanssen 1973; Koutchmy 1977). According to their morphological features and magnetic-field configurations (Uzzo et al. 2006; Vourlidas 2006), the streamer structures can be divided into four regions: (1) cores observed as conical-shaped structures, corresponding to closed field lines, (2) legs located at the outer boundaries of the conical-shaped structures, relating to open field lines surrounding the closed fields, (3) cusps detected between the apexes of the conical-shaped structures and the bases of the long thin rays, connecting to converging open fields above the apexes of the closed fields and below the merging open fields, (4) stalks shown as the long thin rays, referring to plasma sheets generated by merging the open fields. By solving analytic models based on the geometrical properties of magnetic-field lines of streamers with mass and magnetic flux conservations under a magnetohydrostatic equilibrium, several researchers have expected that outward-moving particle flows from the Sun (solar wind streams) might exist along the streamers' legs and stalks (Parker 1964; Newkirk 1967; Pneuman 1968, 1969).

Wang et al. (2007a, 2007b) have carefully investigated several coronal streamers observed on 2003–2006 by using white-light coronagraph images from the Large Angle Spectroscopic CORonagraph (LASCO; Brueckner et al. 1995) C2 on board the Solar and Heliospheric Observatory (SOHO) spacecraft and magnetic-field configurations from Potential Field Source Surface (PFSS) extrapolation. Here, the LASCO-C2 observes outer-

corona structures from 2.0 to $6.0 R_{\odot}$ with a spatial resolution ($11''.4 \text{ pixel}^{-1}$) and specific temporal cadences ($12 \sim 24$ minutes). They find that the coronal streamers can be divided into two types according to their magnetic-field configurations. One type is a typical coronal streamer called a helmet streamer (HS), which overlies closed fields in the inner corona and separates open field lines of opposite magnetic polarity in the outer corona. These opposite-polarity open fields (open bipolar fields) can produce plasma and current sheets as observed by HS stalks. The other type is a pseudo streamer (PS), which overlies twin closed fields in the lower corona and separates open magnetic field lines of the same magnetic polarity. These same-polarity open fields (open unipolar fields) can cause plasma sheets without current sheets as observed by PS stalks. The above HS and PS characteristics are also well identified in global magnetohydrodynamics (MHD) models such as MHD outside A Sphere (MAS) (Riley et al. 2011; Riley & Luhmann 2012). By examining solar wind observations at 1 au and coronal magnetic-field configurations from the PFSS model, several researchers have found the inverse correlation between solar wind speed and the flux-tube expansion factors (Wang & Sheeley 1990; Arge & Pizzo 2000; Fujiki et al. 2015). From these empirical results, it is generally thought that HSs (PSs) having large (small) flux-tube expansion factors can produce slow (fast) solar wind streams.

By using LASCO-C2/C3 and Sun–Earth Connection Coronal and Heliospheric Investigation (Howard et al. 2008) COR2 observations on board the Solar TERrestrial Relations Observatory (STEREO) spacecraft, many researchers have identified localized brightness enhancement structures (blobs) that periodically propagate outward along the streamers' stalks in HSs

(Sheeley et al. 1997, 2009; Wang et al. 1998, 2000; Song et al. 2009; Viall & Vourlidis 2015; Wang & Hess 2018) and PSs (Wang et al. 2007b). In addition to that, Viall & Vourlidis (2015) have observed outward-moving blobs located on and near HS legs as shown in their Figure 1. Following the results of the above studies, the blobs in HSs gradually accelerate from speeds of $0 \sim 100 \text{ km s}^{-1}$ near $3 R_{\odot}$ to speeds of $200 \sim 450 \text{ km s}^{-1}$ near $20 R_{\odot}$. Their mean speeds at different heliocentric distances are similar to the solar wind speeds from Parker’s model (Parker 1958). On the other hand, the speeds of PS blobs are about 200 km s^{-1} near $3 R_{\odot}$, which are larger than the Parker’s solar wind speed. These observational characteristics are also confirmed by several researchers who use the Ultraviolet Coronagraph Spectrometer (UVCS; Kohl et al. 1995) on board SOHO and estimate the outflow speeds of O VI ions in the HSs (Strachan et al. 2002; Frazin et al. 2003; Antonucci et al. 2005; Susino et al. 2008; Abbo et al. 2010) and PSs (Abbo et al. 2015). They find that the outflow speeds are similar to those from streamer blob observations: in HSs, the outflow speeds range from 0 to 100 km s^{-1} at the heights between 1.5 and $5 R_{\odot}$, while they range from 105 to 200 km s^{-1} at the heights between 1.95 to $2.22 R_{\odot}$ in PSs. From these, it is generally believed that outflow streams in HSs (PSs) are a possible source of slow (intermediate or fast) solar winds.

There are several possible formation mechanisms for HS and PS blobs (see Wang et al. 2000, 2007b; Abbo et al. 2016 for reviews). Relating to HS blobs, there are two representative mechanisms. One is releasing of stretched closed loops near a streamer cusp, which has a weak magnetic field that makes it possible for closed loops to expand outward, reconnecting with each other on opposite-polarity magnetic-field configurations, and pinching off (Sheeley et al. 2009; Suess et al. 2009; Wang & Hess 2018). The other is interchange reconnections on same-polarity field configurations between closed loops and their adjacent open fields near a streamer cusp (Sheeley et al. 1997; Wang et al. 1998, 2000; Crooker et al. 2004). These reconnections happen in three-dimensional field configurations and allow trapped streamer materials on the tops of closed loops to escape outward along the open fields. For PS blobs, there are also two possible mechanisms. One is similar to the second mechanism of HS blobs: interchange reconnections between closed loops and adjacent open fields in PSs or open fields rooted in the coronal holes outside PSs (Wang et al. 2007a, 2007b). The other is interchange reconnections on opposite-polarity field configurations between closed loops and adjacent open fields within the fan and spine structures as shown in Figure 17(c) of Abbo et al. (2016) and also in Figure 7 of Crooker et al. (2012).

Since the K-coronagraph (K-Cor) on the Mauna Loa Solar Observatory provides unique inner-corona structures from 1.05 to $3.0 R_{\odot}$ with a high spatial resolution ($5''5 \text{ pixel}^{-1}$) and temporal cadence (15 s), several researchers use it to examine the kinematics and formation mechanism of inner-corona blobs formed in a post-CME ray as well as the origin of outer-corona blobs detected from LASCO-C2 (Cheng et al. 2018; Lee et al. 2020, 2021; Patel et al. 2020; Yu et al. 2020). From these, we think that K-Cor observations are also suitable for estimating the kinematics and formation mechanisms of streamer blobs in the inner corona. In this study, by analyzing two HSs and two PSs observed on 2018 and 2019 in K-Cor and LASCO-C2 observations, we try to investigate formation regions of HS and PS blobs for inferring their possible generation mechanisms. We also examine their propagating speeds for confirming

whether or not HSs (PSs) are related to slow (intermediate or fast) solar wind streams.

This paper is organized as follows. In Section 2, we describe the data and analyses to determine inner and outer-corona streamer blobs and their observational characteristics such as formation regions and propagating speeds. We provide our results and discussion in Section 3. A summary and conclusion are presented in Section 4.

2. Data and Analysis

2.1. Data

K-Cor is a ground-based coronagraph that has observed the inner coronal structure within a limited time window due to geographic and weather conditions during the period from 2013 to the present, while LASCO-C2 is a space-based one that has continuously provided outer corona coverage over the period from 1996 to the present. To select HSs and PSs measured simultaneously from K-Cor and LASCO-C2, we used the Mauna Loa Solar Observatory (MLSO) event table.⁶ This table offers a list of coronal phenomena (e.g., coronal mass ejections and coronal cavities) with their information (e.g., location and observational features) as well as available MLSO data (e.g., K-Cor and Coronal Multichannel Polarimeter, CoMP). The data-selection process of this study can be summarized as follows. (1) To avoid complex coronal structures, we only consider 712 HS and 39 PS candidates from 2018 to 2020 (solar minimum between solar cycles 24 and 25) by filtering keywords such as coronal cavity and pseudo streamer. (2) By visual inspection of the streamer candidates in K-Cor images with their observational features described in the table, we extract 10 HSs and 6 PSs with the following criteria: HS has a large and dark coronal cavity as well as stretched loops in the inner corona, while PS has twin coronal cavities and a narrow plasma sheet (fan and spine structure). These well-observed inner streamer structures of HSs and PSs in K-Cor observations indicate that our extracted HSs and PSs have typical coronal streamer structures and they are located near the plane of the sky, leading to the possibility of projection effects from a single-view observation being negligible. (3) Finally, we select two events for each streamer type satisfying two conditions: first, their magnetic-field configurations from Solar Software PFSS field extrapolations have characteristics similar to those from Wang et al. (2007a, 2007b) as described in Section 1, and second, their outer coronal structures (top of the core, cusp, and stalk) are well identified in LASCO-C2 observations.

Figure 1 shows an example of our selected HS and PS. Panels (a) and (b) show the HS observed on the southeast limb (position angle, PA, $\sim 135^{\circ}$) in 2018 October 24 and the PS detected on the southwest limb (PA $\sim 250^{\circ}$) in 2018 April 12, respectively. Top to bottom rows present their inner coronal structures detected by K-Cor, coronal magnetic-field configurations from the PFSS model, and outer coronal structures from LASCO-C2. The other HS and PS are observed in 2019 August 22 on southeast limb (PA $\sim 130^{\circ}$) and 2019 September 30 on northwest limb (PA $\sim 290^{\circ}$), respectively. As shown in the top panels of Figure 1, HSs and PSs clearly have different inner coronal structures: HSs have stretched loop structures above single coronal cavities, while PSs have fan and spine structures above twin cavities. By contrast, they seem to have

⁶ https://mlso.hao.ucar.edu/mlso_event_table.php/

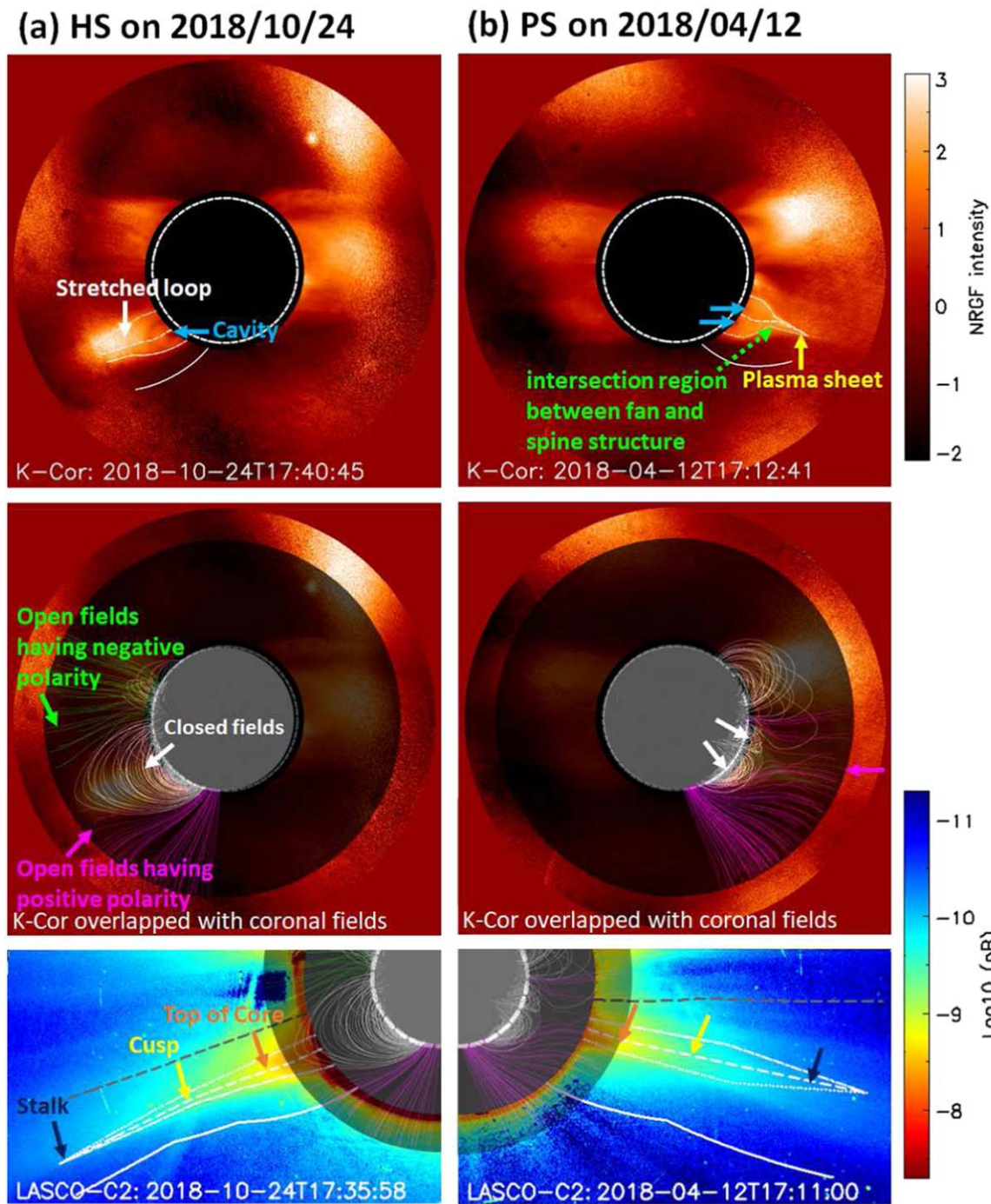


Figure 1. Examples of our selected streamers: (a) HS on the southeast limb in 2018 October 24 and (b) PS on the southwest limb in 2018 April 12. Top to bottom rows show the K-Cor images applied using the NRGF technique, K-Cor images overlaid coronal magnetic-field configuration images from PFSS extrapolation, and LASCO-C2 images overlaid with the coronal fields. The FOV of the LASCO-C2 images is 512×300 pixels. In the K-Cor images, blue, white, yellow, and green arrows indicate the dark cavity, stretched loop, plasma sheet, and intersection region between the fan and spine structure of each selected streamer. The white dashed and black circles represent the location and size of the solar disk and the K-Cor occulting disk. In the coronal magnetic-field images, white, green, and purple arrows show the closed fields, open magnetic fields having negative and positive polarities related to each selected streamer. In the LASCO-C2 images, orange, yellow, and dark blue arrows represent the apparent top of the core, cusp, and stalk, respectively. In the top and bottom panels, white and gray lines represent non-radial specific slits used to plot spacetime diagrams. More detailed description of the slits are provided in Section 2.2.

similar outer coronal structures such as a cusp and stalk as shown in the bottom panels. When we check SDO/AIA 304 Å images from the Korean Data Center (KDC) for SDO,⁷ we find that all our streamers have bright prominences at their bases near the cavities. This finding together with the well-observed

inner and outer streamer structures imply that our selected streamers are located on the plane of sky. From this, we simply assume that the projection effects are negligible when we estimate the kinematics of streamer blobs in our streamers.

For determining inner and outer-corona blobs for each streamer, we use K-Cor level-2.0 and LASCO-C2 level-1.0 data, respectively. They are suitable for quantitative scientific analysis

⁷ <http://sdo.kasi.re.kr>

and taken from the K-Cor online database⁸ and the virtual solar observatory via Solar Software, respectively. We note that the K-Cor database provides 15 s and an average of 2 minutes of data. In this study, we use the 2 minutes of data because they have a relatively higher signal-to-noise ratio on coronal structures than the 15 s data. The noise is mainly produced by aerosol particles in the atmosphere that blow in front of the telescope (J. T. Burkepil 2021, private communication).

2.2. Determination of Streamer Blobs and Their Kinematic Characteristics

To identify inner-corona streamer blobs (K-Cor streamer blobs), we take the following procedure. (1) During the K-Cor observational period for each event, we produce K-Cor intensity and Normalizing Radial Graded Filter (NRGF) images by applying the NRGF technique (Morgan et al. 2006) to the intensity images. When we compare the two images, we find that the NRGF images show more detailed streamer structures (e.g., coronal cavities and stretched loops) than the intensity ones. We also make their running-difference images with an interval of 12 minutes, which is the same as the LASCO-C2 temporal cadence. (2) We transform the images into polar coordinates (r, θ) with a size of 164×3600 , where 164 and 3600 are the pixel sizes of the heliocentric distances (from 1.1 to $2.0 R_{\odot}$ with an interval of about $0.006 R_{\odot}$) and position angles (PAs, from $0^{\circ}0$ to $360^{\circ}0$ with an interval of $0^{\circ}1$), respectively. (3) Considering the possible blob-formation mechanisms as described earlier in Section 1, we generate spacetime plots of K-Cor intensity and running-difference images along the non-radial specific slits. The slits are located on the centers of stretched loops or their east- and westside outer boundaries in the HSs shown as white dashed, dotted, and dashed-dotted lines in the top left panel of Figure 1. These are used for determining whether HS blobs appeared (or formed) in the HS center and leg regions. Here, the eastside (westside) outer boundary means the specific locations whose position angles are smaller and larger than those of each streamer center. In PSs, the slits are situated on intersection regions between the fan and spine structures or the outer boundaries of the fan structures, which are shown as white lines in the top right panel of Figure 1. These are used to estimate PS blobs generated in the intersection regions and legs of PSs. Here, we note that for increasing signal-to-noise ratio of streamer blobs, the slits are taken to be 5 pixels wide ($0^{\circ}5$) in the PA directions and we use their average values. (4) The detailed selection process of streamer blobs can be summarized as follows. By visual inspection of the running-difference spacetime plots, we select localized brightness enhancement trajectories having positive (or negative) slopes, which are the candidates of outward-moving (or sunward-moving) streamer blobs. Checking whether or not the selected trajectories are the real signatures of streamer blobs, we make a background spacetime plot along the slit that is located on a background region (far from more than 10° , 100 pixels, in the PA directions compared to streamer structures), shown as a solid line in the top panels of Figure 1, and compare it with the spacetime plots in streamer structures. If the selected trajectories only exist in the spacetime plots on streamer structures, we define them as streamer blobs. On the other hand, if they exist in both the spacetime plots in and far from streamer structures and they are similar to each other, we regard them as artifact structures.

For outer-corona streamer blobs (LASCO-C2 streamer blobs), we use the following procedure: (1) During the one-day period of LASCO-C2 for each event, we make LASCO-C2 background-subtracted images. To do this, we generate a monthly minimum image by using 30 images observed near 00:00 UT in the last 30 days before each event. Then, we subtract the monthly minimum image from intensity images on each event. Since the outer streamer structures (e.g., cusp and stalk) are well shown in the LASCO-C2 background-subtracted images, we use them and their running-difference images, making an interval of 60 minutes, which is generally used for examining LASCO-C2 streamer blobs (Wang et al. 2000; Wang & Hess 2018). (2) We transform the images into polar coordinates (r, θ) with a size of 340×3600 , where 340 and 3600 are the pixel sizes of heliocentric distances (from 2.0 to $6.2 R_{\odot}$ with an interval of about $0.012 R_{\odot}$) and PAs, respectively. (3) We make spacetime plots along the non-radial specific slits. The slits are located on the centers of streamers' cores, cusps, and stalks or their outer boundaries as shown by the white lines in the bottom panels of Figure 1. These are used for determining HS and PS blobs formed in the streamer center and leg regions. (4) We use the same blob-selection process as described above. It should be noted that the temporal cadences of K-Cor and LASCO-C2 spacetime plots are set as 2 and 12 minutes to easily estimate the speeds of streamer blobs in their spacetime plots. For this, we make their virtual time tables and image arrays with 2 and 12 minute cadences during their observational periods. We select the closest images before or after the time table and store them in the virtual image arrays, which are used to make the spacetime plots.

For our selected streamer blobs, we examine their observational characteristics. By visual inspection of streamer structures and their associated blob locations in spacetime plots of intensity and running-difference images, we examine the formation regions of streamer blobs. By investigating their spacetime data, we estimate the propagating speeds of streamer blobs by using linear fittings.

It should be noted that although inner coronal structures of HSs and PSs are well identified in K-Cor observations, as shown in the top panels of Figure 1, K-Cor has a limitation for determining inner-corona streamer blobs by analyzing the spacetime plots of K-Cor images for our selected events. When we carefully compare spacetime plots of K-Cor running-difference images obtained in and far from streamer structures, we find that localized brightness enhancement structures exist in all spacetime plots and they are similar to each other. This means that the localized brightness enhancement structures in K-Cor running-difference images might be artificial structures, which could be caused by the brightness of artifacts produced by atmospheric aerosols higher than that of inner-corona streamer blobs. Since K-Cor has the limitation of streamer blob observations, we cannot show results about kinematics and formation mechanisms of inner-corona streamer blobs in this paper. We will only show the observational characteristics of HS and PS blobs measured from LASCO-C2. Even though K-Cor has the limitation, it provides whether or not streamer structures observed in LASCO-C2 are located on the plane of the sky by investigating the inner-corona structures as described in Section 2.1. Therefore, by analyzing our selected K-Cor and LASCO-C2 data, we can inspect the similarity and dissimilarity of LASCO-C2 blob features observed in HSs with

⁸ https://mlso.hao.ucar.edu/mlso_data_calendar.php?calinst=kcor

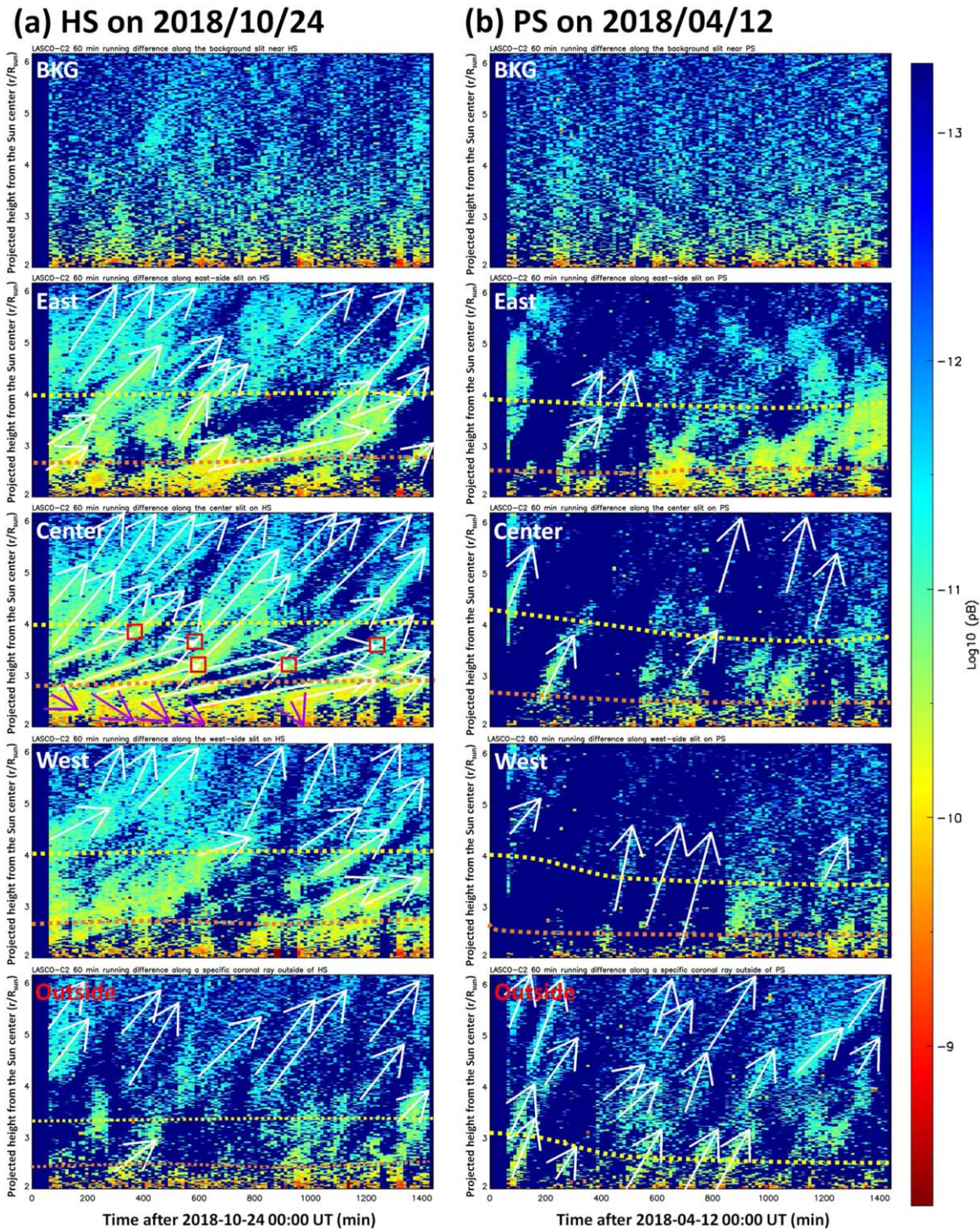


Figure 2. Spacetime plots of LASCO-C2 running-difference images along the background (first row), eastside (second row), center (third row), westside (fourth row), and outside slits (fifth row) on the HS and PS presented in Figure 1. White and purple arrows represent outward- and sunward-moving streamer blob trajectories, respectively. Their slopes imply linear speeds during the durations. The horizontal orange and yellow lines indicate the apparent tops of streamer core and cusp regions on each slit. Red boxes indicate the specific heights showing the sudden slope change of each blob trajectory (sudden speed jump).

and without the inner coronal structures. These will be presented in Section 3.5.

3. Results and Discussion

Figure 2 shows examples of spacetime plots of LASCO-C2 running-difference images along the non-radial specific slits on the HS and PS presented in the bottom panels of Figure 1. By

visual inspection of the spacetime plots, streamer blobs (white and purple arrows) are clearly observed in the LASCO-C2 running-difference images. We also find that the trajectories of the streamer blobs can be fitted by linear regression lines during their durations. Based on the investigations of these spacetime plots for our selected streamer events, we show the appearance and formation regions and outward-moving speeds of LASCO-C2 HS and PS blobs in the following sub-sections.

3.1. Outward-moving Blobs along the Centers and Legs of HSs and PSs

By analyzing the spacetime plots of LASCO-C2 running-difference images along the non-radial specific slits for our selected HSs and PSs, we observe outward-moving blobs along the centers and legs of HSs and PSs shown as white arrows in the second to fourth rows of panels of Figure 2. In order to check whether or not our observed blobs at a specific time are individual blobs having different locations, we carefully examine the LASCO-C2 running difference at the heights between 2 and $5 R_{\odot}$, which are related to streamer core, cusp, and leg regions as well as the base of stalk. At a height above $5 R_{\odot}$, the streamer stalk, the positions of non-radial specific slits are close to each other, making it hard to distinguish blob propagation paths. Figure 3 shows examples of our observed HS and PS blobs detected in LASCO-C2 running-difference images. From these, we find that almost all HS blobs are individual blobs in different positions such as the eastside leg, center, and westside leg of HSs as shown with blue, red, and green arrows of Figure 3(a), while a few blobs having wider angular widths than angular distances between two different slits can be shown in two spacetime plots along the slits. For examples, blobs indicated as orange (brown) arrows can be detected in the spacetime plots along the eastside and center (center and westside) slits on HSs. When we examine PS blobs, we find that all PS blobs are individual blobs having different locations such as PS centers and legs as shown in Figure 3(b). We also find that although outward-moving HS and PS blobs have irregular and different shapes that make it hard to estimate their general morphology, they seem to have elongated structures parallel to the streamers. Our results demonstrate that streamer blobs persistently propagate outward along (1) the centers of HSs and PSs and (2) their legs until the base of the stalk. The first finding is similar to previous observations using LASCO (Sheeley et al. 1997; Wang et al. 1998, 2000, 2007b; Song et al. 2009; Wang & Hess 2018) and STEREO-COR2 (Viall & Vourlidas 2015), while the second finding is similar to the result of Viall & Vourlidas (2015) who investigated 10 days of white-light images from the STEREO-COR2 from 2008 January 14 to 23 and found outward-moving blobs located on and near HS legs as shown in their Figure 1.

When we trace the streamer blobs up to $6 R_{\odot}$, we find that the blobs seem to converge into streamer stalks. In order to estimate daily blob-occurrence rates for each streamer type, we measure blobs passing at the height of $5 R_{\odot}$ in HS and PS centers. From this we find that mean values of HS and PS blob-occurrence rates for our selected streamers are about 9 and 4, respectively. Interestingly, we also observe outward-moving blobs along the specific coronal ray outside of HSs and PSs shown as gray arrows in Figure 3. When we examine their spacetime plot as shown in the fifth row of panels in Figure 2, we find that the HS and PS blobs propagate outward about 8 and 6 times a day. The different blob-occurrence rates between the insides and outsides of PSs might be caused by relatively low coronal brightness of streamer regions located outside of PSs that lead to more easily detected outward-moving blobs because the LASCO-C2 instrument has a limitation of brightness sensitivities.

3.2. Formation Regions of HS and PS Blobs

By careful investigation of the spacetime plots of LASCO-C2 intensity and running-difference images for the HSs and PSs, we

find the following observational characteristics: (1) On the centers of HSs, bidirectional moving blobs (outward- and sunward-moving blobs) are frequently observed at an average height of ($2.55 R_{\odot}$) below the tops of streamer cores ($2.80 R_{\odot}$). These outward- and sunward-moving blobs are indicated as white and purple arrows at the heights between 2 and $3 R_{\odot}$ in the third row of panels in Figure 2(a). (2) Along the legs of HSs and their outsides, there seem to be only outward-moving blobs as shown in the second, fourth, and fifth row of panels in Figure 2(a). (3) PSs generally have outward-propagating blobs along their centers, legs, and outsides as shown in the second to fifth rows of Figure 2(b). These results demonstrate that HS blobs along the streamer centers are formed below the tops of streamer cores at the height of $2.6 R_{\odot}$, while the other HS and PS blobs are made at or below $2.0 R_{\odot}$. Our finding about the blob-formation regions of HS centers is similar to the suggestion from in situ measurements by Suess et al. (2009) and Weberg et al. (2012) who have estimated the density ratios of heavy ions to proton such as helium-to-proton (He/H), oxygen-to-proton (O/H), and iron-to-proton (Fe/H) ratios by analyzing Ulysses and ACE data. They have compared the estimated ratios with those from streamer cores by SOHO/UVCS (Raymond et al. 1997) and found a similarity between them. From this, they proposed the idea that streamer materials observed in heliospheric current sheets might originate in the streamer core. However, this finding is different from that of previous LASCO-C2 observations (Sheeley et al. 1997; Wang et al. 1998, 2000; Wang & Hess 2018) which generally show that HS blobs form at the streamer cusp.

From our observational results, together with possible blob-formation mechanisms as described earlier in Section 1, we can infer that HS blobs along the streamer centers (legs and outsides of HSs) are generated by the releasing of stretched closed loops below the tops of streamer cores caused by plasma pressure gradients in high-plasma beta conditions of the HS centers, expanding the closed loops outward, reconnecting with each other on opposite-polarity magnetic-field configurations, and pinching off (interchange reconnections on same-polarity field configurations between closed loops and their adjacent open fields). For PS blobs along the streamer centers and legs, two representative mechanisms are possible. One is interchange reconnection on same-polarity field configurations between closed loops and adjacent open fields in PSs or open fields rooted in the coronal holes outside PSs. The other is interchange reconnection on opposite-polarity field configurations between closed loops and adjacent open fields within the fan and spine structures. Its height might be about $1.5 R_{\odot}$ as shown by the green dotted arrows in the top panel of Figure 1(b). Regarding to formation of PS blobs along the specific rays outside of PSs, the PS blobs might be generated by interchange reconnection on same-polarity field configurations between open fields of PSs and closed loops outside PSs. To make it clear for estimating formation mechanisms of blobs along the HS legs and all PS blobs, it is necessary to further investigate using inner coronal observations such as solar eclipses, STEREO-COR1, and Solar Orbiter-Metis (Antonucci et al. 2020).

3.3. Outward-moving Speeds of HS and PS Blobs

Figures 4(a) and (b) ((c) and (d)) show speed–height plots for outward-moving HS (PS) blobs observed on 2018 October 24 and 2019 August 22 (2018 April 12 and 2019 September 30), respectively. Here, blue, red, green, and gray symbols show the blob speeds along the eastside leg, center, westside

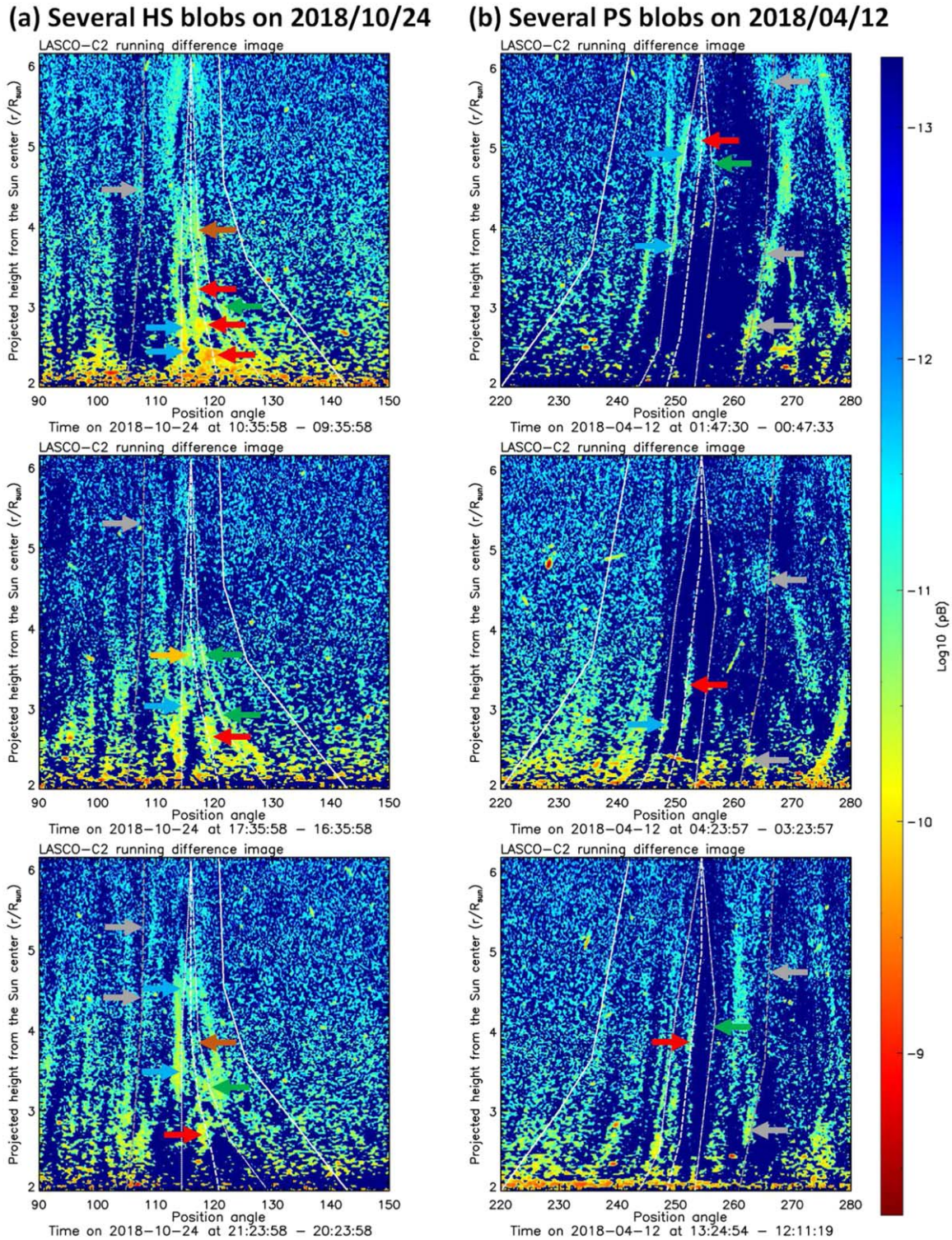


Figure 3. In panel (a), examples of outward-moving HS blobs along the eastside, center, westside, and outside of the HS, observed on 2018 October 24 at 10:36, 17:36, and 21:24 UT, respectively (top to bottom). These blobs are shown as blue, red, green, and gray arrows, and they are previously identified as white arrows in the spacetime plots of Figure 2(a). The orange (brown) arrow indicates an HS blob shown in both the eastside and center (center and westside) slits because its angular width is larger than the angular distance between two slits. In panel (b), we present PS blobs observed on 2018 April 12 at 1:47, 4:24, and 13:25 UT, respectively. The blue, red, green, and gray arrows are the same as those in panel (a). These blobs are identified as white arrows in Figure 2(b). The non-radial specific slits are the same as those in the bottom panels of Figure 1.

leg, and outside of each streamer structure. From these, we find that the speeds of outward-moving HS blobs are generally similar to or smaller than the solar wind speed based on Parker’s model (1958) as shown in panels (a) and (b), while the

PS blob speeds are larger than the Parker’s solar wind speed and smaller than the solar wind speed based on the coronal hole given by Chandra & Hollweg (2009) in panels (c) and (d). Assuming that outward-moving HS and PS blobs can be taken

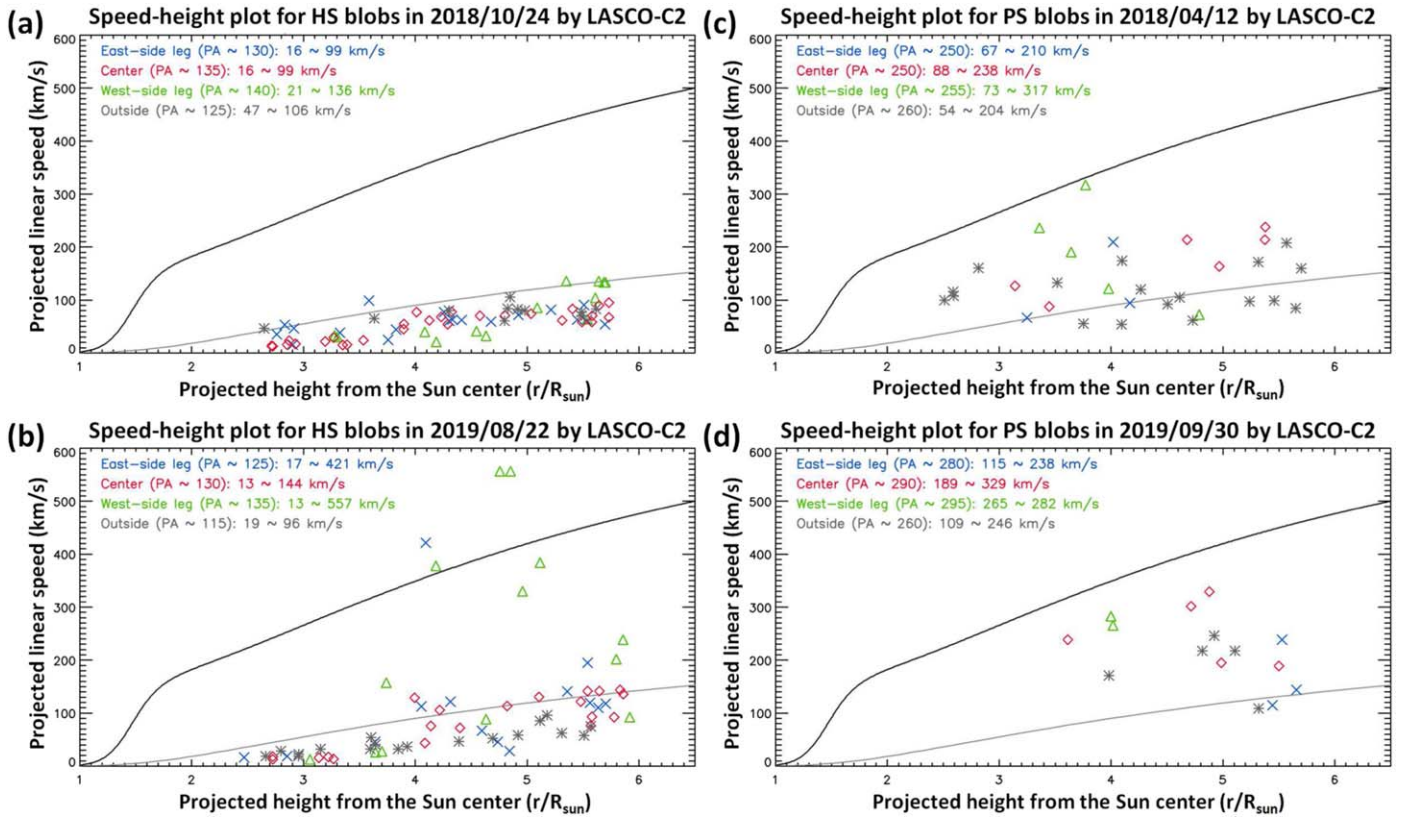


Figure 4. Left panel: speed–height plots for HS blobs observed in 2018 October 24 and 2019 August 22 ((a) and (b)), and right panel: PS blobs in 2018 April 12 and 2019 September 30 ((c) and (d)). Blue, red, green, and gray symbols indicate the linear speeds of streamer blobs at their average heights along the eastside, center, westside, and outside of each streamer structure, respectively. The black and gray lines represent the solar wind speeds based on coronal hole given by Chandra & Hollweg (2009) and Parker’s model (1958).

as tracers of solar wind speeds in the region of HSs and PSs (Sheeley et al. 1997; Song et al. 2009), our results demonstrate that HSs and PSs are possible sources of slow and intermediate solar winds, respectively. Our findings are similar to the results from previous coronagraph measurements in HSs (Sheeley et al. 1997; Wang et al. 1998, 2000; Song et al. 2009; Viall & Vourlidas 2015; Wang & Hess 2018) and PSs (Wang et al. 2007b).

When we carefully compare blob speeds between different propagating regions of each streamer, we find the following characteristics: (1) HS and PS blob speeds are a little bit different depending on the propagating regions such as streamer centers and legs. For example, HS blob speeds along the streamer center range from 13 to 144 km s⁻¹, which is slightly smaller than those along the streamer legs (from 13 to 238 km s⁻¹ except for extreme cases having larger 300 km s⁻¹). For PS blobs, those on streamer centers range from 88 to 329 km s⁻¹, which is larger than those on streamer legs (from 67 to 317 km s⁻¹). (2) The blob speeds inside streamer structures (centers and legs) are larger than outside ones closer to the solar equator. For example, HS blob speeds inside streamer structures range from 13 to 238 km s⁻¹, which is larger than those on their outsides (from 19 to 106 km s⁻¹). For PS blobs, those on the insides range from 67 to 329 km s⁻¹, which is larger than those on their outsides (from 54 to 246 km s⁻¹). The first finding about the different speed distributions between streamer centers and the legs of each streamer type might be explained by the expansion-factor model (Wang & Sheeley 1990; Arge & Pizzo 2000; Fujiki et al. 2015), which is based on inverse correlation between the flux-tube expansion factors and solar wind speeds. For HSs, the regions of streamer centers have relatively

larger flux-tube expansion factors than those of streamer legs as estimated from Figure 2 of Riley & Luhmann (2012), leading to solar wind speeds of streamer centers that are relatively smaller than those of streamer legs. For PSs, the regions of the streamer center have smaller expansion factors than those of the streamer legs, resulting in solar wind speeds of streamer centers that are larger than those of the streamer legs. These processes can make different blob speeds depending on the streamer regions inside HSs and PSs. The second finding about the different speed distributions between the inside and outside located toward the solar equator of each streamer structure is similar to typical solar wind speed distributions at solar minimums (McComas et al. 2003; Bemporad 2017; Cho et al. 2018). The differences in PS blob speeds between the inside and outside can be described by the expansion model because the expansion factors on the insides are smaller than those on the outsides. However, it is hard to explain the differences of HS blob speeds between the inside and outside. To make it clear for the generation mechanisms of different speed distributions between the inside and outside, it is necessary to further investigate by using MHD models such as MAS (Riley et al. 2011; Riley & Luhmann 2012). It should be noted that we cannot rule out the possibilities that the different speed distributions are caused by either the multiple streamers under the single current sheet as shown in Figure 5 of Wiegmann et al. (2000) or multiple current sheets by complex magnetic fields as shown in Figure 2 of Maiewski et al. (2020). In addition to that, we find that although the relative locations from the solar equator of HSs (PSs) observed in 2018 and 2019 are similar to each other, HS (PS) blob speeds are a little bit greater in 2019 compared to 2018. In order to determine conclusively

whether or not blob speeds are dependent on solar cycles, we need further investigations by using more events.

3.4. Sudden Speed Jumps of HS Blobs in Streamer Cusps

By carefully examining the HS blob trajectories along the streamer centers for the 2 HSs observed in 2018 October 24 and 2019 August 22, we find sudden changes in the slopes of blob trajectories in spacetime plots of LASCO-C2 running-difference images as shown in the blue boxes of Figure 2(a). We plot their speed–height plots as shown in Figure 5. We also present average heights of the tops of the streamer core and cusp during the observational period for each event as shown in vertical orange and yellow lines, respectively. From these, we find that the average speeds of HS blobs in 2018 October 24 suddenly jump from $\langle 19 \rangle$ to $\langle 63 \rangle$ km s⁻¹ in the streamer cusp ($\langle 3.57 R_{\odot} \rangle$), while those in 2019 August 22 unexpectedly increase from $\langle 15 \rangle$ to $\langle 58 \rangle$ km s⁻¹ in the streamer cusp ($\langle 3.52 R_{\odot} \rangle$). Our results first demonstrate that HS blobs undergo a large acceleration process in the specific heights of streamer cusp regions. These sudden speed jumps of HS blobs might be caused by the sunward magnetic tension forces of overlying stretched closed fields and/or bidirectional (outward and sunward) outflows generated by the magnetic reconnection process in the streamer cusps. Figure 5(c) shows a proposed schematic model for the formation of the sudden speed jumps of the HS blobs. Initially, an HS blob (vertically elongated red ellipse) is formed by the releasing of stretched closed loops below the tops of streamer cores and it propagates outward as shown in the left panel. During its propagation, the blob is constantly affected by the sunward tension forces (wide purple arrow), which decrease its outward motions. In addition to that, the sunward outflows (wide gray arrow) via a Y-type magnetic reconnection process (explosion symbol) can further decelerate its outward motions. Therefore, the speed of the HS blob is slow until the cusp as shown in the middle panel. After the blob arrives at the top of the cusp, the tension force is not affected. However, it is accelerated by the outward outflows (wide black arrow). The blob speed rapidly increases as shown in the right panel. These processes can cause the sudden speed jumps of HS blobs in the streamer cusps.

3.5. Similarity and Dissimilarity of Blob Features Observed in HSs with and without Clear Inner Coronal Structures

In order to check the similarity and dissimilarity of observational characteristics of blobs appearing in the HSs with and without clear inner coronal structures (dark coronal cavity and stretched loops), we examine two western HSs (PA $\sim 270^{\circ}$) in 2018 October 24 and 2019 August 22 by using the same analysis. These HSs do not have clear inner coronal structures as shown in top panel of Figure 1(a). By investigating the HSs, we find similar statistical trends. Blobs move outward along the centers and legs of HSs. Their speeds are generally similar to the Parker’s solar wind speed. Blob speeds along the streamer centers range from 6 to 197 km s⁻¹, which is slower than those along the streamer legs (from 15 to 298 km s⁻¹). Blobs seem to converge into streamer stalks and their daily occurrence rates at a height of $5 R_{\odot}$ are about 6. These results, together with our findings described in the above sections, demonstrate that all HSs persistently release their associated blobs in the centers and legs of the HSs, and they are possible sources of slow solar winds. However, we find the

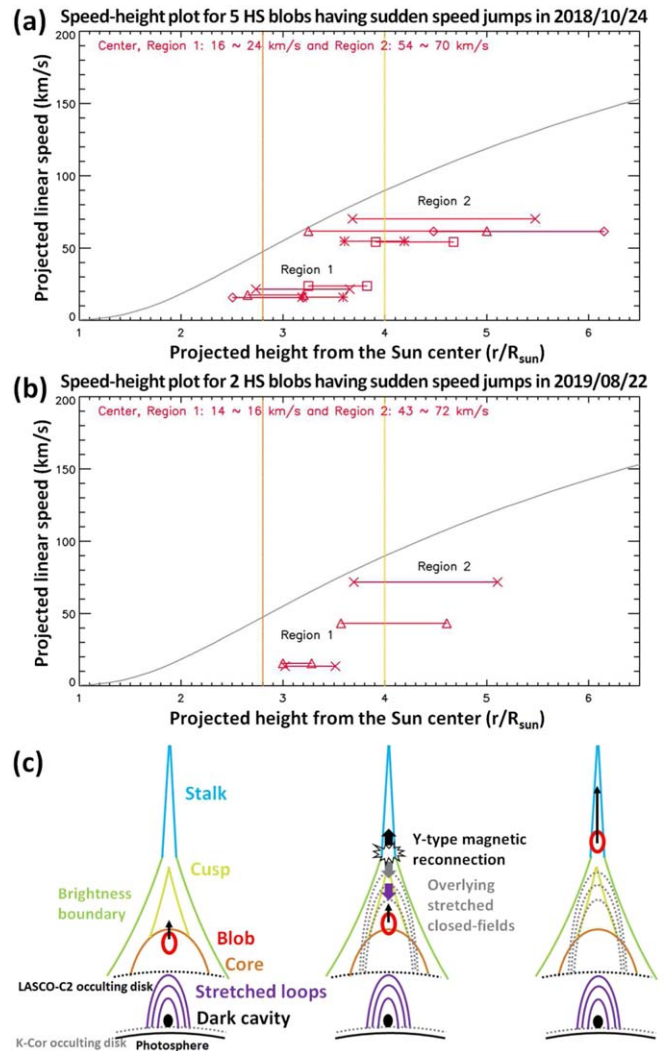


Figure 5. Speed–height plots of several HS blobs having sudden speed jumps observed on HSs in 2018 October 24 (a) and 2019 August 22 (b). Different symbols indicate different HS blobs. The first and second symbols of each blob show its initial and final appearance heights during propagation with the same outward-moving speed. The vertical orange and yellow lines indicate the average heights of the tops of the streamer core and cusp during the observational period for each event. The gray lines are the same as those in Figure 4. In panel (c), we present a schematic explanation of the formation of the sudden speed jumps of HS blobs along the streamer centers. Left panel: initial stage, showing the observed location and apparent motion of an HS blob formed below the top of a streamer core. Middle panel: middle stage, representing the apparent motion of the HS blob, sunward tension forces (wide purple arrow) of overlying stretched closed fields, and bidirectional outflows (wide gray and black arrows) generated by Y-type magnetic reconnection processes. Right panel: late stage, indicating the apparent motion of the HS blob. The length of each black arrow indicates the speed of the HS blob. More detailed descriptions are provided in the text.

following different trends. Blobs along the streamer centers seem to form at average heights of $\langle 3.0 R_{\odot} \rangle$ near or above the tops of streamer cores ($\langle 2.90 R_{\odot} \rangle$), which is similar to the previous LASCO-C2 observations (Sheeley et al. 1997; Wang et al. 1998, 2000; Wang & Hess 2018). It is hard to find the sudden speed jumps of HS blobs because there are no blobs having clear trajectories from streamer core to streamer cusp regions. These results indicate that observational formation regions and kinematics of HS blobs along the HS centers might be changed depending on the relative positions of HSs along the line-of-sight direction.

4. Summary and Conclusion

In this study, we examine two helmet and two pseudo streamers (HSs and PSs) observed in 2018 and 2019 by using K-Cor and LASCO-C2 observations for understanding formation mechanisms of localized brightness enhancement structures (blobs) observed in HSs and PSs as well as confirming whether or not HSs (PSs) are possible sources of slow (intermediate or fast) solar wind streams. Our streamer events satisfy the following observational criteria: HSs have dark coronal cavities and stretched loop structures at their bases and PSs have twin coronal cavities and narrow plasma sheets, which are well observed in K-Cor observations. Their outer-corona structures (top of the core, cusp, and stalk) are well identified in LASCO-C2 observations. These well-observed inner and outer streamer structures indicate that our streamers are located on the plane of sky and projection effects are negligible when we estimate kinematics of streamer blobs in our streamers.

Through careful investigations of K-Cor and LASCO-C2 images for our events, we find the following observational features. (1) Although inner coronal streamer structures are well identified in K-Cor observations, their associated blobs are not because of artifacts produced by atmospheric aerosols. (2) Blobs detected in LASCO-C2 persistently move outward along the centers of HSs and PSs as well as their legs until the base of the stalk. They eventually converge into streamer stalks. We also detect outward-moving blobs along the specific coronal rays outside of the HSs and PSs. (3) Blobs along the HS centers are formed at average heights of ($2.6 R_{\odot}$) below the tops of the streamer cores ($2.8 R_{\odot}$), while blobs along the legs of HSs and their outsides as well as PS blobs might be generated at or below $2.0 R_{\odot}$. (4) The speeds of outward-moving HS blobs are generally similar to or smaller than the solar wind speed based on Parker's model (1958), while the speeds of outward-moving PS blobs are larger than the Parker's solar wind speed and smaller than the solar wind speed based on coronal holes given by Chandra & Hollweg (2009). (5) Interestingly, HS (PS) blob speeds along the streamer centers are slightly smaller (larger) than those along the streamer legs, which might be explained by the expansion-factor model (Wang & Sheeley 1990; Arge & Pizzo 2000; Fujiki et al. 2015). The blob speeds inside streamer structures (centers and legs) are larger than outside ones closer to the solar equator, which is similar to typical solar wind speed distributions at solar minima (McComas et al. 2003; Bemporad 2017; Cho et al. 2018). (6) Several HS blobs along the streamer centers show sudden speed jumps in streamer cusps, implying that HS blobs undergo a large acceleration process in the specific heights of streamer cusp regions. These might be caused by the sunward magnetic tension force of overlying stretched closed fields and/or bidirectional (sunward and outward) outflows generated by the magnetic reconnection process in the streamer cusps. From these findings, we can infer that HS blobs along the streamer centers are generated by the following formation mechanism: the releasing of stretched closed loops below the tops of streamer cores, expanding the closed loops outward, reconnecting with each other on opposite-polarity magnetic-field configurations, and pinching off. This formation mechanism is similar to the suggestion from in situ measurements by Suess et al. (2009) and Weberg et al. (2012). To estimate the formation mechanisms of blobs along the legs of HSs and their outsides and PS blobs, we need further investigations using inner coronal observations such as solar eclipses, STEREO-COR1, and Solar Orbiter-Metis


(Antonucci et al. 2020). We also deduce that HSs and PSs are possible sources of slow and intermediate solar winds under the assumption that outward-moving HS and PS blobs can be taken as tracers of solar wind speeds in the regions of HSs and PSs. These findings are similar to the results from previous coronagraph measurements in HSs (Sheeley et al. 1997; Wang et al. 1998, 2000; Song et al. 2009; Viall & Vourlidas 2015; Wang & Hess 2018) and PSs (Wang et al. 2007b). To make it clear for the generation mechanisms of different speed distributions between the inside and outside, it is necessary to further investigate using MHD models such as MAS (Riley et al. 2011; Riley & Luhmann 2012).

In addition to that, Korea Astronomy and Space Science Institute (KASI) in collaboration with NASA Goddard Space Flight Center (GSFC) are developing a next-generation coronagraph called as COronal Diagnostic EXperiment, (Cho et al. 2017), which will simultaneously observe the electron density, temperature, and speed structures of solar coronal streamers from about 3.0 to 8.0 Rs. By using CODEX together with the Solar Orbiter-Metis, we will understand the physical conditions in different solar wind regions and find their generation mechanisms.

We are grateful to the referee, associate editor, and scientific editor for helpful and constructive comments. This research is supported by the Korea Astronomy and Space Science Institute under the R&D program Development of a Solar Coronagraph on the International Space Station (Project No. 2021-1-850-09) supervised by the Ministry of Science, ICT, and Future Planning. This research is also supported by the Basic Science Research Program through the National Research Foundation of Korea (NRF) funded by the Ministry of Education (2019R1F1A1055071). J.A. is supported by the Basic Science Research Program through the NRF funded by the Ministry of Education (2020R111A1A01072337). H.L. is supported by an NRF grant funded by the Korean government (MSIT) 2020R1C1C1008102). P.K. is supported by NASA's Heliophysics Guest Investigator (80NSSC20K0265) programs. We thank the SOHO/LASCO CME catalog for providing LASCO-C2 images, the virtual solar observatory for LASCO-C2 data, and the K-Cor online database for the K-Cor images and data (DOI:10.5065/D69G5JV8). The CME catalog is generated and maintained at the CDAW Data Center by NASA and The Catholic University of America in cooperation with the Naval Research Laboratory. The SOHO/LASCO data used here are produced by a consortium of the Naval Research Laboratory (USA), Max-Planck-Institut für Sonnensystemforschung (Germany), Laboratoire d'Astronomie (France), and the University of Birmingham (UK). SOHO is a project of international cooperation between the ESA and NASA. The K-Cor data are courtesy of the Mauna Loa Solar Observatory, operated by the High Altitude Observatory, as part of the National Center for Atmospheric Research (NCAR). NCAR is supported by the National Science Foundation. The SDO data were provided by the Korea Data Center (KDC) for SDO in cooperation with NASA, which was supported by the "Development of Korea Space Weather Research Center" project of the Korea Astronomy and Space Science Institute (KASI).

ORCID iDs

Jae-Ok Lee  <https://orcid.org/0000-0002-7652-7883>

Kyung-Suk Cho  <https://orcid.org/0000-0003-2161-9606>

Junmo An  <https://orcid.org/0000-0001-7899-1746>
 Hwanhee Lee  <https://orcid.org/0000-0001-8669-2906>
 Jungjoon Seough  <https://orcid.org/0000-0002-1723-5944>
 Yeon-Han Kim  <https://orcid.org/0000-0001-5900-6237>
 Pankaj Kumar  <https://orcid.org/0000-0001-6289-7341>

References

- Abbo, L., Antonucci, E., Dodero, M. A., et al. 2010, *AdSpR*, **46**, 1400
 Abbo, L., Lionello, R., Riley, P., et al. 2015, *SoPh*, **290**, 2043
 Abbo, L., Ofman, L., Antiochos, S. K., et al. 2016, *SSRv*, **201**, 55
 Antonucci, E., Abbo, L., & Dodero, M. A. 2005, *A&A*, **435**, 699
 Antonucci, E., Romoli, M., Andretta, V., et al. 2020, *A&A*, **642**, A10
 Arge, C. N., & Pizzo, V. J. 2000, *JGR*, **105**, 10465
 Bemporad, A. 2017, *ApJ*, **846**, 86
 Brueckner, G. E., Howard, R. A., Koomen, M. J., et al. 1995, *SoPh*, **162**, 357
 Chandra, B. D. G., & Hollweg, J. V. 2009, *ApJ*, **707**, 1659
 Cheng, X., Li, Y., Wan, L. F., et al. 2018, *ApJ*, **866**, 64
 Cho, K.-S., Bong, S.-C., Choi, S., et al. 2017, *JKAS*, **50**, 139
 Cho, I. H., Moon, Y. J., Nakariakov, V. M., et al. 2018, *PhRvL*, **121**, 075101
 Crooker, K. N., Antiochos, S. K., & Zhao, X. 2012, *JGR*, **117**, A04104
 Crooker, K. N., Huang, C. L., Lamassa, S. M., et al. 2004, *JGR*, **109**, A03107
 Frazin, R. A., Cranmer, S. R., & Kohl, J. L. 2003, *ApJ*, **597**, 1145
 Fujiki, K., Tokumaru, M., Iju, T., et al. 2015, *SoPh*, **290**, 2491
 Howard, R. A., Moses, J. D., Vourlidas, A., et al. 2008, *SSRv*, **136**, 67
 Kohl, J. N., Esser, R., Gardner, L. D., et al. 1995, *SoPh*, **162**, 313
 Koutchmy, S. 1977, in *Illustrated Glossary for Solar and Solar-Terrestrial Physics*, ed. A. Bruzek & C. J. Durrant (Dordrecht: Reidel), 39
 Lee, J. O., Cho, K. S., Lee, K. S., et al. 2020, *ApJ*, **892**, 129
 Lee, J. O., Cho, K. S., Nakariakov, V. M., et al. 2021, *JKAS*, **54**, 61
 Maiewski, E. V., Malova, H. V., Kislov, R. A., et al. 2020, *CosRe*, **58**, 411
 McComas, D. J., Elliott, H. A., Schwadron, N. A., et al. 2003, *GeoRL*, **30**, 1517
 Morgan, H., Habbal, S. R., & Woo, R. 2006, *SoPh*, **236**, 263
 Newkirk, G., Jr. 1967, *ARA&A*, **5**, 213
 Parker, E. N. 1958, *ApJ*, **128**, 664
 Parker, E. N. 1964, *ApJ*, **139**, 690
 Patel, R., Pant, V., Chandrasekhar, K., et al. 2020, *A&A*, **644**, A158
 Pneuman, G. W. 1968, *SoPh*, **3**, 578
 Pneuman, G. W. 1969, *SoPh*, **6**, 255
 Raymond, J. C., Kohl, J. L., Noci, G., et al. 1997, *SoPh*, **175**, 645
 Riley, P., Lionello, R., & Linker, J. A. 2011, *SoPh*, **274**, 361
 Riley, P., & Luhmann, J. G. 2012, *SoPh*, **277**, 355
 Saito, K., & Tandberg-Hanssen, E. 1973, *SoPh*, **31**, 105
 Sheeley, N. R., Jr., Lee, D. H., Casto, K. P., et al. 2009, *ApJ*, **694**, 1471
 Sheeley, N. R., Jr., Wang, Y. M., Hawley, S. H., et al. 1997, *ApJ*, **484**, 472
 Song, H. Q., Chen, Y., Liu, K., et al. 2009, *SoPh*, **258**, 129
 Strachan, R., Suleiman, R., Panasyuk, A. V., et al. 2002, *ApJ*, **571**, 1008
 Suess, S. T., von Ko, Y. K., Steiger, R., et al. 2009, *JGR*, **114**, A04103
 Susino, R., Ventura, R., Spadaro, D., et al. 2008, *A&A*, **488**, 303
 Uzzo, M., Strachan, L., Vourlidas, A., et al. 2006, *ApJ*, **645**, 720
 Viall, N. M., & Vourlidas, A. 2015, *ApJ*, **807**, 176
 Vourlidas, A. 2006, in *IAU Symp. 233, Solar Activity and its Magnetic Origin*, ed. V. Bothmer & A. A. Hady (Cambridge: Cambridge Univ. Press), 197
 Wang, Y.-M., Biersteker, J. B., Sheeley, N. R., et al. 2007a, *ApJ*, **660**, 882
 Wang, Y. M., & Hess, P. 2018, *ApJ*, **859**, 135
 Wang, Y. M., & Sheeley, N. R., Jr. 1990, *ApJ*, **355**, 726
 Wang, Y.-M., Sheeley, N. R., Jr., & Rich, N. B. 2007b, *ApJ*, **658**, 1340
 Wang, Y. M., Sheeley, N. R., Jr., Socker, D. G., et al. 2000, *JGR*, **105**, 25133
 Wang, Y. M., Sheeley, N. R., Jr., Walters, J. H., et al. 1998, *ApJL*, **498**, L165
 Weberg, M. J., Zurbuchen, T. H., & Lepri, S. T. 2012, *ApJ*, **760**, 30
 Wiegmann, T., Schindler, K., & Neukirch, T. 2000, *SoPh*, **191**, 391
 Yu, S., Chen, B., Reeves, K., et al. 2020, *ApJ*, **900**, 17